Controlled Fabrication of Hierarchically Structured Nitrogen-Doped Carbon Nanotubes as a Highly Active Bifunctional Oxygen Electrocatalyst

*Xianglong Zhao, Feng Li, Ruining Wang, Jeong-Min Seo, Hyun-Jung Choi, Sun-Min Jung, Javeed Mahmood, In-Yup Jeon, and Jong-Beom Baek**

Hierarchically structured nitrogen-doped carbon nanotube (NCNT) composites, with copper (Cu) nanoparticles embedded uniformly within the nanotube walls and cobalt oxide (Co_xO_y) nanoparticles decorated on the nanotube surfaces, are fabricated via a combinational process. This process involves the growth of Cu embedded CNTs by low- and high-temperature chemical vapor deposition, post-treatment with ammonia for nitrogen doping of these CNTs, precipitation-assisted separation of NCNTs from cobalt nitrate aqueous solution, and finally thermal annealing for Co_xO_y decoration. Theoretical calculations show that interaction of Cu nanoparticles with CNT walls can effectively decrease the work function of CNT surfaces and improve adsorption of hydroxyl ions onto the CNT surfaces. Thus, the activities of the oxygen reduction reaction (ORR) and the oxygen evolution reaction (OER) are significantly enhanced. Because of this benefit, further nitrogen doping, and synergistic coupling between Co_xO_y and NCNTs, Cu@NCNT/Co_xO_y composites exhibit ORR activity comparable to that of commercial Pt/C catalysts and high OER activity (outperforming that of IrO_2 catalysts). More importantly, the composites display superior long-term stability for both ORR and OER. This simple but general synthesis protocol can be extended to design and synthesis of other metal/metal oxide systems for fabrication of high-performance carbon-based electrocatalysts with multifunctional catalytic activities.

1. Introduction

The oxygen reduction reaction (ORR) and oxygen evolution reaction (OER), both of which are sluggish in nature, play pivotal roles in renewable energy technologies including fuel cells, metal/air batteries, and water splitting.[1,2] Platinum- and ruthenium (or iridium)-based materials generally make the most active ORR[3] and OER catalysts,[4,5] respectively, but the prohibitive cost and relative scarcity of these catalyst materials hinder their practical use in large-scale applications. To date, substantial efforts have been dedicated to the design of various cost-effective alternatives, such as perovskites,[6] spinels,[7] heteroatom (e.g., nitrogen, sulfur, and boron) doped/codoped carbon nanotubes (CNTs),[8,9] graphene,[10–12] or carbon nanosheets,[13,14] and CNTs or graphene supported transition-metal oxide, such as manganese (Mn) oxide[15,16] and iron (Fe) oxide.[17,18] It has been reported that nitrogen-doped CNT (NCNT) supported cobalt oxide nanoparticles possessed excellent ORR catalytic activity. This was because: (1) CNTs had large surface area and excellent electrical conductivity; (2) nitrogen doping changed the charge density and distribution within CNTs; and (3) CNTs had synergistic coupling effects with cobalt oxide nanoparticles.[19] However, the improvement of ORR activity in these developed NCNT/cobalt oxide composites was hindered by the intrinsically low ORR activity of CNTs. Also, the growth of cobalt oxide nanoparticles on NCNT surfaces involved time-consuming multistep procedures as well as the extra preoxidation of CNT surfaces, and the latter required the use of strong and dangerous oxidants. Recently, Bao and co-workers reported that ORR activity of CNTs was enhanced effectively by encapsulating Fe nanoparticles within CNTs. This was because the interaction of Fe nanoparticles with CNT walls reduced the work function at surfaces of the CNTs, making CNT surfaces more active for ORR.[20] Similar to Fe, copper (Cu) is also an earth-abundant and inexpensive transition-metal element. More importantly, the work of Zhang and co-workers proved that Cu had inherent ORR catalytic activity.[21] Therefore, it would be highly desirable to introduce interaction between CNT walls and Cu nanoparticles

Dr. X. Zhao
Key Laboratory of Materials Physics
Anhui Key Laboratory of Nanomaterials and Nanotechnology
Institute of Solid State Physics
Chinese Academy of Sciences
Hefei 230031, P. R. China

Dr. X. Zhao, Dr. F. Li, J.-M Seo, Dr. H.-J Choi, S.-M. Jung, Dr. J. Mahmood, Dr. I.-Y. Jeon, Prof. J.-B. Baek
School of Energy and Chemical Engineering/Center for Dimension-Controllable Organic Frameworks
Ulsan National Institute of Science and Technology (UNIST)
UNIST 50, Ulsan 44919, Republic of Korea
E-mail: jbbaek@unist.ac.kr

Dr. R. Wang
Hebei Key Laboratory of Optic-Electronic Information and Materials
College of Physics Science and Technology
Hebei University
Baoding 071002, P. R. China

DOI: 10.1002/adfm.201605717

for NCNT/cobalt oxide composites, to afford high ORR activity. However, to the best of our knowledge, there has not yet been a report on such a study.

Here, by rationally performing consecutive low- and high-temperature chemical vapor deposition (CVD) of carbon layers on anodic aluminum oxide (AAO) pore walls loaded with copper nitrate, we fabricated CNTs where walls were uniformly embedded with Cu nanoparticles (hence, we denoted these CNTs as Cu@CNTs). Then, by post-treatment of Cu@CNTs in ammonia to achieve nitrogen doping (Cu@NCNTs), precipitation-assisted separation of Cu@NCNTs from cobalt nitrate aqueous solution, and the following thermal annealing, we realized selective decoration of cobalt oxide (Co_xO_y) nanoparticles on Cu@NCNT surfaces. Density functional theory (DFT) calculations revealed that interaction of Cu nanoparticles with CNT walls induced decreased work function of CNT surfaces and improved adsorption of hydroxyl ions onto the CNT surfaces. Because of these outstanding benefits, further nitrogen doping, and synergistic coupling between Co_xO_y nanoparticles and Cu@NCNTs, the Cu@NCNT/Co_xO_y composites demonstrated high ORR activity comparable to that of commercial Pt/C catalysts, OER activity higher than that of IrO_2 catalysts, and excellent durability for ORR/OER in alkaline solution. Furthermore, this approach was extended to the fabrication of different metal/metal oxide composites with similar hierarchical structures.

2. Results and Discussion

Figure 1a shows the fabrication process of Cu@CNTs. Specifically, copper nitrate was first loaded on AAO pore walls by immersing AAO in copper nitrate aqueous solution and drying it. Then, low- and high-temperature CVD processes were conducted at 450 and 800 °C, respectively, with acetylene as a carbon precursor. According to our previous work,[22] accumulated deposition of carbon deriving from pyrolysis of acetylene at 450 °C onto surfaces of transition-metal nanoparticles led to encapsulation of transition-metal nanoparticles within carbon layers. This was because transition-metal nanoparticles lost their catalytic effects on CNT growth at low temperature (<500 °C).[23,24] Therefore, during CVD at 450 °C, copper oxide nanoparticles that resulted from thermal decomposition of copper nitrate were first reduced to Cu nanoparticles by carbon and hydrogen (from pyrolysis of acetylene), and then encapsulated within carbon layers. Moreover, our previous work also showed that only a small quantity of acetylene was pyrolyzed at 450 °C.[22] Hence, the CVD at 450 °C resulted in negligible carbon deposition on the AAO pore walls (Figure S1, Supporting Information). It has been reported that the amount of pyrolyzed acetylene increased dramatically after the increase of the temperature.[22] Therefore, a large number of carbon layers were deposited on the AAO pore walls after CVD at 800 °C. In this case, the original carbon-layer-encapsulated Cu nanoparticles (formed at 450 °C) were further covered by the additional carbon layers formed at 800 °C, leading to complete embedment of Cu nanoparticles within carbon layers on the AAO pore walls. It is well known that carbon layers deposited on AAO pore walls duplicated perfectly AAO pore morphology.[25–27] Hence, after the CVD at 800 °C, the carbon layers duplicated cylindrical morphology of AAO pores, resulting in the formation of Cu nanoparticles embedded CNTs, i.e., Cu@CNTs.

Figure 1b is a scanning electron microscope (SEM) image of Cu@CNTs, showing that many hollow Cu@CNTs with almost uniform diameters have been achieved. Figure 1c is a transmission electron microscope (TEM) image of a typical Cu@CNT, revealing that Cu@CNT has uniform wall thickness and its diameter is ≈85 nm, which is consistent with that of AAO.[22] In addition, Figure 1c shows that many Cu nanoparticles with size <10 nm are uniformly distributed inside the Cu@CNT. From the high-resolution TEM (HRTEM) image (Figure 1d), we can see that these Cu nanoparticles are actually embedded within CNT walls which are ≈2.5 nm thick. The inset in Figure 1d shows an HRTEM image of a Cu nanoparticle, showing that it is well crystallized, and its interplanar *d*-spacing is ≈0.18 nm, which agrees well with that of Cu [200] planes. Hence, this result confirms that this nanoparticle is made of Cu. The X-ray diffraction (XRD) pattern (Figure 1e) of the Cu@CNTs shows three remarkable Cu peaks at 43.3°, 50.3°, and 52.0°, corresponding to the [111], [200], and [420] planes, respectively. Hence, XRD results also verify that the nanoparticles embedded in the CNT walls are composed of Cu.

To shed light on the importance of combination of low- and high-temperature CVD for the formation of Cu@CNTs, we performed only high-temperature CVD, which is commonly used for growth of CNTs inside the AAO template,[25,28] after loading the AAO pore walls with copper nitrate. As shown in Figure 1f, the synthesized Cu@CNTs have very thin walls, whose thickness cannot be distinguished in the TEM image. In addition, there are many curly CNTs with small diameters (≈10 nm), which were formed by Cu catalysis, inside the CNTs (as marked by red arrows). This result is consistent with the previous report that some Cu nanoparticles loaded on AAO pore walls could catalyze the growth of small-diameter CNTs via the vapor–liquid–solid mechanism.[29] As growth of these small-diameter CNTs required a large number of carbon deposited on the surfaces of Cu nanoparticles, we think this reduced the amount of carbon deposited on the AAO pore walls, and eventually resulted in the formation of Cu@CNTs with thin walls (Figure 1g). In addition, we found that Cu@CNTs achieved by only high-temperature CVD suffered from the poor structural integrity. As shown in Figure 1f and Figure S2a (Supporting Information), even brief ultrasonication for the preparation of TEM specimen can seriously damage thin walls of these Cu@CNTs to nearly break apart. Therefore, in comparison with only high-temperature CVD, the combination of low- and high-temperature CVD is beneficial for the production of robust Cu@CNTs with thick walls.

It was reported that CNTs precipitated easily in water, because their density was greater than that of water.[30] Hence, after dispersing pure CNTs fabricated using bare AAO (Figure S2b, Supporting Information) and the Cu@CNTs in water, we observed the precipitation of both (**Figure 2**a). More importantly, we found that Cu@CNTs precipitated more rapidly than pure CNTs. As shown in Figure 2a, after dispersion in water for 2 min, almost all the Cu@CNTs have precipitated to the bottom, while many pure CNTs are still suspended in the water. We attributed this to the embedding of Cu nanoparticles,

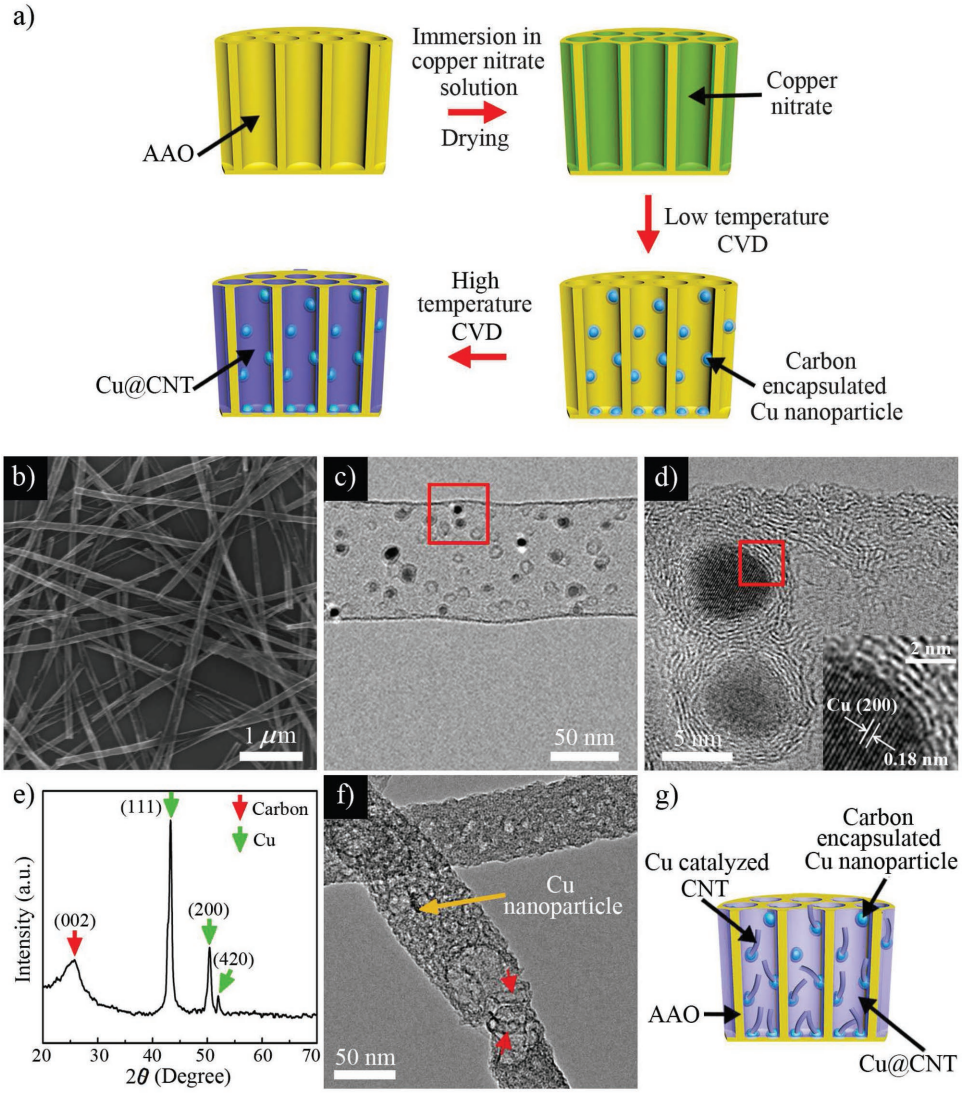

Figure 1. a) Schematic representation of the fabrication process of Cu@CNTs. b) The SEM image of Cu@CNTs. c) The TEM image of a Cu@CNT. d) The HRTEM image taken from the square area marked in part (c). Inset: The HRTEM image taken from the square area. e) The XRD pattern of Cu@CNTs. f) The TEM image of Cu@CNTs produced by only high-temperature CVD. The two red arrows indicate the Cu catalyzed CNTs. g) Schematic representation of AAO and the Cu@CNTs achieved by only high-temperature CVD.

which resulted in Cu@CNTs with higher density than the pure CNTs. For the same reason, we also observed rapid precipitation of Cu@NCNTs (fabricated via ammonia post-treatment of Cu@CNTs at 900 °C[31]) in cobalt nitrate aqueous solution (Figure S3, Supporting Information). Then, after sucking away the solution, we obtained easy separation of Cu@NCNTs, which were still encapsulated by the residual cobalt nitrate aqueous solution (Figure 2b). According to the previous report, aqueous solution could not infuse into inner spaces of the CNTs because of the hydrophobic CNT walls.[32] This revealed that cobalt nitrate aqueous solution only coated surfaces of the Cu@NCNTs. Hence, after drying these Cu@NCNTs to prepare cobalt nitrate loaded on their surfaces, and then annealing to make cobalt nitrate decomposed to Co_xO_y, we achieved Cu@NCNT/Co_xO_y composites, where Co_xO_y nanoparticles were selectively decorated on Cu@NCNT surfaces (Figure 2c). Figure 2d,e shows a SEM and a TEM image, respectively, of the Cu@NCNT/Co_xO_y composites, demonstrating clearly that Co_xO_y nanoparticles are outside of the NCNTs. From the HRTEM images (Figure 2f,g), we can see that Cu nanoparticles are embedded within the NCNT walls and meanwhile high crystallinity Co_3O_4 nanoparticles of ≈7 nm are decorated on the NCNT surface. The XRD pattern (Figure 2h) of the Cu@NCNT/Co_xO_y composites shows four Co_xO_y peaks at 31.1°, 36.4°, 42.4°, and 61.4°, which are assigned to Co_3O_4 [220], CoO [101], CoO [200], and CoO [220], respectively. Hence, XRD results confirm that the Co_xO_y nanoparticles on NCNT surfaces are composed of both Co_3O_4 and CoO. X-ray photoelectron spectroscopy (XPS) spectrum (Figure 2i) of the Cu@NCNT/Co_xO_y composites suggests the presence of C, Cu, N, Co, and O, and their estimated weight percentages are 67.5, 4.0, 3.3, 5.0, and 20.0 wt%, respectively (Table S1, Supporting

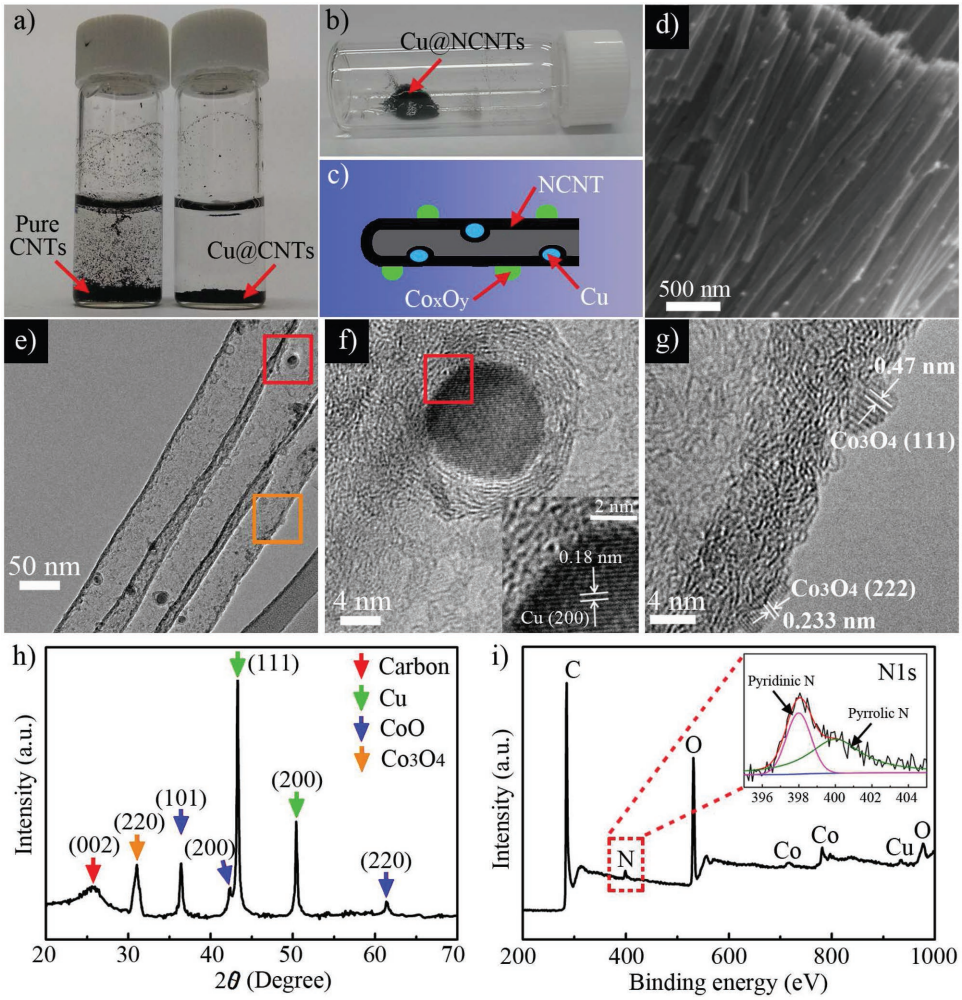

Figure 2. a) Photograph of pure CNTs and Cu@CNTs after dispersion in water for 2 min. b) Photograph of Cu@NCNTs separated from cobalt nitrate aqueous solution. c) Schematic representation of a Cu@NCNT/Co_xO_y composite. d) The SEM image of Cu@NCNT/Co_xO_y composites. e) The TEM image of three overlapped Cu@NCNT/Co_xO_y composites. f,g) HRTEM images taken from the red and brown square areas in part (e), respectively. Inset in part (f): The HRTEM image taken from the red square area. h,i) XRD and XPS spectra of Cu@NCNT/Co_xO_y composites, respectively. The inset in part (i) is a high-resolution XPS spectrum of N 1s.

Information). The high-resolution XPS spectrum of N 1s (inset of Figure 2i) shows that there are two types of nitrogen (i.e., pyridinic N, ≈398.0 eV and pyrrolic N, ≈400.0 eV) in the Cu@NCNT/Co_xO_y composites,[16] and the high-resolution XPS spectrum of Cu 2p3/2 (Figure S4, Supporting Information) reveals that there are Cu–N species (≈933.5 eV) in the composites besides metallic Cu (≈932.2 eV).[33] Therefore, ammonia post-treatment of Cu@CNTs achieved both nitrogen doping of carbon layers and formation of Cu–N species. In addition, the inductively coupled plasma optical emission spectrometry (ICP-OES) measurement was further used to examine the amounts of metal elements in the Cu@NCNT/Co_xO_y composites, and weight percentages of Cu and Co are ≈5.0 and ≈5.3 wt%, respectively. Figure S5a (Supporting Information) shows the nitrogen adsorption–desorption isotherm of the Cu@NCNT/Co_xO_y composites, showing a distinct hysteresis loop under the relative pressure ranging from 0.45 to 1.0. This result suggests the presence of mesopores in the Cu@NCNT/Co_xO_y composites. The pore size distribution curve (Figure S5b, Supporting Information) demonstrates a sharp peak at a half pore width of ≈2.6 nm, confirming again the presence of mesopores. The Brunauer–Emmett–Teller (BET) surface area of the composites is ≈391 m^2 g^{-1}, and their pore volume is ≈1.096 cm^3 g^{-1}. Hence, the BET surface area of the composites is remarkably larger than that (154 m^2 g^{-1}) of the previously reported Co_3O_4/NCNT composites.[19] We think that the result could be attributed to the low weight percentage of metal (metal oxide) in the Cu@NCNT/Co_xO_y composites. In addition, this result could be ascribed to the gases deriving from thermal decomposition of cobalt nitrate, which blow and separate the originally agglomerated Cu@NCNTs.[34]

Using DFT calculations, we obtained electrostatic potential profiles of single-wall CNT (SWCNT)(6,6) and Cu_4@SWCNT(6,6), where a Cu_4 cluster was inside the SWCNT(6,6) and decorated on its wall. As shown in **Figure 3**a, the work functions at the surfaces of SWCNT(6,6) and Cu_4@SWCNT(6,6) are ≈4.05 and ≈3.37 eV, respectively, indicating that interaction of Cu_4 clusters with the SWCNT wall induces a remarkable decrease in work

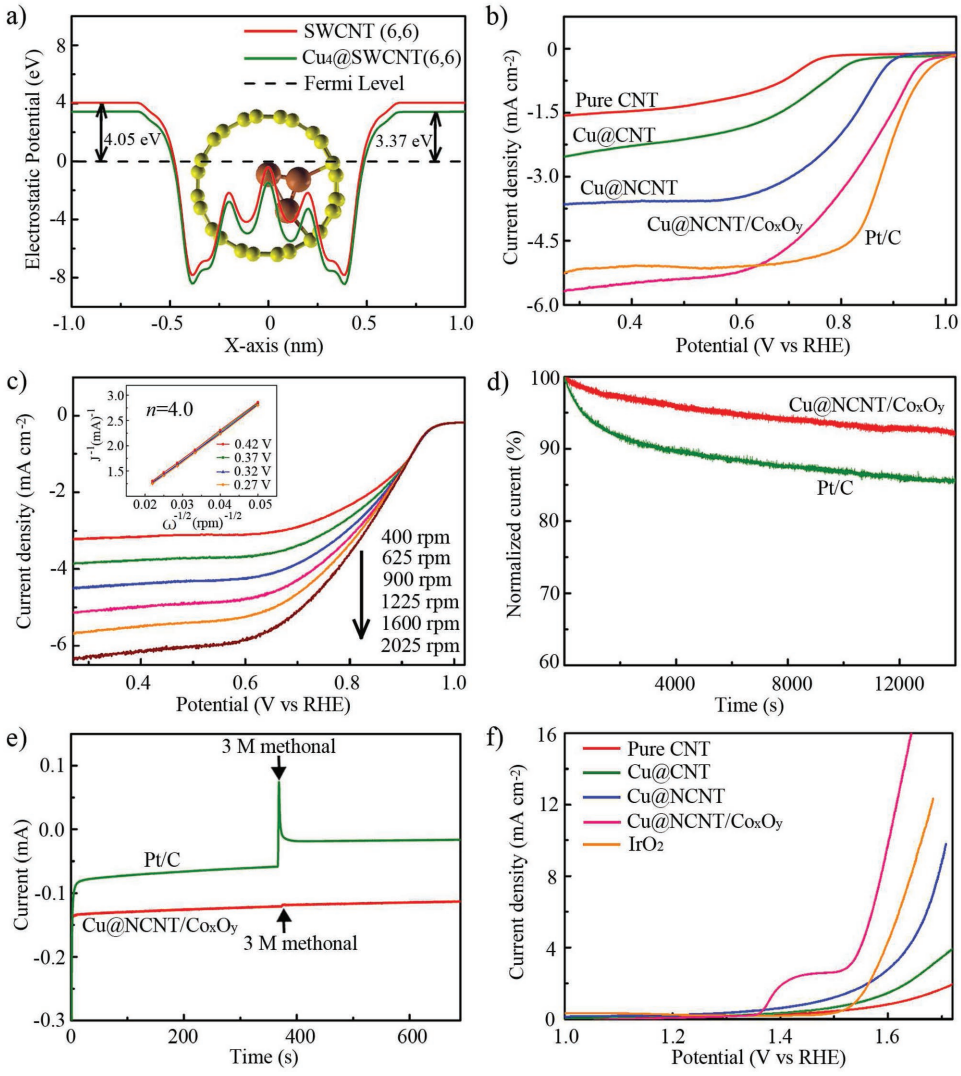

Figure 3. a) Electrostatic potential profiles averaged on the plane perpendicular to the *X*-axis as a function of the *X*-axis of the supercell of SWCNT and Cu_4@SWCNT. The schematic representation of Cu_4@SWCNT is shown in the background. As indicated, the work functions at the surfaces of SWCNT(6,6) and Cu_4@SWCNT(6,6) are ≈4.05 eV and ≈3.37 eV, respectively. b) LSVs of pure CNTs, Cu@CNTs, Cu@NCNTs, Cu@NCNT/Co_xO_y composites, and Pt/C (scan rate: 0.01 V s^{-1}; rotation rate: 1600 rpm). c) LSVs of Cu@NCNT/Co_xO_y composites at different rotation rates (scan rate: 0.01 V s^{-1}). Inset: K–L plots at different potentials. d) Chronoamperometric response of Cu@NCNT/Co_xO_y composites and Pt/C in oxygen saturated 0.1 M aq. KOH solution at 0.72 V. e) Chronoamperometric response of Cu@NCNT/Co_xO_y composites and Pt/C in oxygen saturated 0.1 M aq. KOH solution at 0.57 V. About 3 M methanol was added at about 360 s. f) LSVs of pure CNTs, Cu@CNTs, Cu@NCNTs, Cu@NCNT/Co_xO_y composites, and IrO_2 (scan rate: 0.01 V s^{-1}; rotation rate: 1600 rpm).

function at the surface of the SWCNT. Also, the work function (≈3.45 eV) at the surface of the double-wall CNT [(DWCNT)(6,6)/(11,11)] is larger than that (≈3.05 eV) at the surface of Cu_4@DWCNT(6,6)/(11,11), where a Cu_4 cluster is decorated on the inner wall of the DWCNT(6,6)/(11,11) (Figure S6, Supporting Information). These results reveal that the interaction of Cu nanoparticles with the CNT walls leads to decrease in work function at the CNT surfaces. The previous work of Bao and coworkers confirmed that such a decrease was able to improve the ORR activity of the CNTs.[20] Hence, the interaction of Cu nanoparticles with the CNT walls is expected to result in better ORR activity for CNTs. Furthermore, our DFT calculations reveal that, in comparison with the surface of SWCNT(6,6), it is energetically more favorable for hydroxyl ions to be adsorbed onto the surface of Cu_4@SWCNT(6,6). This is because adsorption free energy (≈3.73 eV) of hydroxyl ions on the surface of Cu_4@SWCNT(6,6) is remarkably larger than that (≈2.02 eV) on the surface of SWCNT(6,6). Similarly, the adsorption of hydroxyl ions onto the surface of Cu_4@DWCNT(6,6)/(11,11) is more favorable (adsorption free energy: ≈1.39 eV) than onto the surface of DWCNT(6,6)/(11,11) (adsorption free energy: ≈0.42 eV). This reveals that the interaction between Cu nanoparticles and CNT walls may also induce the enhanced OER activity of the CNTs, because easy adsorption of hydroxyl ions onto the catalyst surfaces favors the enhanced OER activity.[2,35] Therefore, these results indicate that our Cu@CNTs, with Cu nanoparticles embedded entirely within

the CNT walls, may have better bifunctional ORR/OER catalytic activity than do the pure CNTs. It was evidenced that both pyridinic N and pyrrolic N, metal-N species, and synergistic coupling between Co_xO_y nanoparticles and carbon nanomaterials, benefited the improvement of ORR/OER activity of carbon nanomaterials.[8,19,35–38] Hence, ORR/OER activity of the Cu@CNTs is expected to increase even more after nitrogen doping and the final Co_xO_y decoration.

In order to examine the ORR activity of pure CNTs, Cu@CNTs, Cu@NCNTs, and Cu@NCNT/Co_xO_y composites, we measured their linear sweep voltammograms (LSVs, Figure 3b) in oxygen saturated 0.1 M aq. KOH solution using rotating disk electrodes at 1600 rpm. As expected, the ORR activity of the Cu@CNTs (onset potential: ≈0.84 V vs the reversible hydrogen electrode (RHE); limiting current density at 0.27 V: ≈−2.54 mA cm^{-2}) is better than that (≈0.77 V, ≈−1.55 mA cm^{-2}) of the pure CNTs, confirming that embedding Cu can improve the ORR activity of CNTs. In addition, Cu@CNTs have a more negative onset potential and a lower limiting current density than do Cu@NCNTs (≈0.89 V, ≈−3.64 mA cm^{-2}). As mentioned above, all of pyridinic N, pyrrolic N, and metal–N species are beneficial for the improvement of ORR activity of the carbon nanomaterials. Therefore, the higher ORR activity of Cu@NCNTs than that of Cu@CNTs could be attributed to each of the pyridinic N, pyrrolic N, and Cu–N species. Also, the possible contribution of Cu–N species to ORR activity of the Cu@NCNTs is revealed by the better ORR activity of Cu@NCNTs than that of the pure NCNTs (Figure S7, Supporting Information). In comparison with Cu@NCNTs, Cu@NCNT/Co_xO_y composites exhibit a more positive onset potential (≈0.95 V) and a higher limiting current density (≈−5.66 mA cm^{-2}). This reveals that the synergistic coupling effect between Co_xO_y nanoparticles and Cu@NCNTs is responsible for the higher ORR activity of the Cu@NCNT/Co_xO_y composites than Cu@NCNTs, because Co_xO_y alone has rather poor ORR activity.[37,39] According to the work of Dai and co-workers,[19] both CoO and Co_3O_4 have synergistic coupling with NCNTs, leading to similar onset potentials for NCNT/CoO and NCNT/Co_3O_4 composites during ORR. However, in comparison with NCNT/Co_3O_4 composites, NCNT/CoO composites exhibited higher ORR current density owing to their smaller charge transfer resistance. Hence, for Co_xO_y nanoparticles consisting of both CoO and Co_3O_4, the composition of CoO could contribute more than that of Co_3O_4 to the high ORR activity of the Cu@NCNT/Co_xO_y composites. Furthermore, the high ORR activity of the Cu@NCNT/Co_xO_y composites confirms that although our method of decorating Co_xO_y nanoparticles on Cu@NCNT surfaces is rather simple, it can still achieve strong coupling between Co_xO_y nanoparticles and Cu@NCNTs. Therefore, our approach is superior to the previously reported methods for fabrication of such NCNT/metal oxide (or CNT/metal oxide) composites in terms of low cost, time saving, and environmental compatibility.[15,19,40] Moreover, Figure 3b also shows that the onset potential of the Cu@NCNT/Co_xO_y composites is very close to that (≈0.97 V) of commercial Pt/C catalysts, together with their limiting current density having a higher value (limiting current density for Pt/C is ≈−5.26 mA cm^{-2}). Thus, Cu@NCNT/Co_xO_y composites have ORR catalytic activity similar to that of Pt/C catalysts.

As high ORR activity of the Cu@NCNT/Co_xO_y composites is closely related to each component of Cu, nitrogen, and Co_xO_y, we think that there could be several active sites for ORR for the Cu@NCNT/Co_xO_y composites. For Fe nanoparticles embedded in CNTs, it has been reported that CNT surfaces with Fe nanoparticles sitting below are active sites for ORR.[20] This is because these surfaces have lower work function due to the interaction between carbon layers and Fe nanoparticles. As the interaction between carbon layers and Cu nanoparticles can also result in reduced work function of CNT surfaces, we think CNT surfaces of the Cu@NCNT/Co_xO_y composites, under which there are Cu nanoparticles, can also serve as active sites to expedite oxygen reduction. It is well known that carbon atoms adjacent to the doped nitrogen atoms become active sites for ORR upon doping of CNTs or graphene, because they have the high charge density.[8,10] On the other hand, many previous reports demonstrate that metal–N species are also active sites to catalyze the ORR.[19,36] As ammonia post-treatment of Cu@CNTs could achieve not only nitrogen doping of CNTs but also the formation of Cu–N species, both carbon atoms adjacent to the doped nitrogen atoms and Cu–N species could be additional active sites for ORR in the Cu@NCNT/Co_xO_y composites. Furthermore, previous researches confirm that cobalt oxide species at the interface between cobalt oxide and carbon nanomaterials are ORR active sites for cobalt oxide decorated carbon nanomaterials.[19,41] Hence, for Cu@NCNT/Co_xO_y composites, where Co_xO_y nanoparticles were decorated on the Cu@NCNT surfaces, Co_xO_y species at the interface between Co_xO_y and Cu@NCNTs could be other ORR active sites.

To gain further insights into the ORR kinetics of the Cu@NCNT/Co_xO_y composites, we measured their LSVs at different rotation rates in oxygen saturated 0.1 M aq. KOH solution. From Figure 3c, we can see that the limiting current density of the Cu@NCNT/Co_xO_y composites increases with the increase of rotation rate. Then, using these LSVs at different rotation rates, we calculated Koutecky–Levich (K–L) plots (J^{-1} vs $\omega^{-1/2}$) at different potentials for the Cu@NCNT/Co_xO_y composites. As shown in the inset of Figure 3c, the K–L plots at all potentials have excellent linearity and almost coincide. This reveals the first-order ORR kinetics at the surfaces of Cu@NCNT/Co_xO_y composites as well as the similar electron transfer number at different potentials during ORR. On the basis of slopes of these K–L plots, we calculated the electron transfer number (n) per oxygen molecule in ORR for Cu@NCNT/Co_xO_y composites to be close to 4. This indicates that ORR processes at the surfaces of the Cu@NCNT/Co_xO_y composites are an ideal four-electron process, which is similar to the case in Pt/C catalysts.[11,19] Using similar approaches, we also obtained electron transfer numbers of ≈3.9, ≈3.0, and ≈2.0 for Cu@NCNTs (Figure S8, Supporting Information), Cu@CNTs (Figure S9, Supporting Information), and pure CNTs (Figure S10, Supporting Information), respectively. Therefore, the ORR processes at the surfaces of Cu@NCNTs are close to the ideal four-electron process, while those at the surfaces of Cu@CNTs and pure CNTs are a mixed two- and four-electron process and a typical two-electron process, respectively.

Because stability and selectivity toward ORR are important parameters for evaluation of ORR catalysts in fuel cells,[15] we studied the long-term durability of Cu@NCNT/Co_xO_y

composites via chronoamperometric measurement at 0.72 V in oxygen saturated 0.1 M aq. KOH solution. As shown in Figure 3d, after running for 12 000 s, current density for the Cu@NCNT/Co_xO_y composites retains more than 90% of the initial value, while that for Pt/C catalysts drops to ≈85% of its initial value. Therefore, Cu@NCNT/Co_xO_y composites have better long-term stability for ORR than do Pt/C catalysts. Next, we examined tolerance to methanol crossover for Cu@NCNT/Co_xO_y composites via the addition of 3 M methanol in 0.1 M aq. KOH solution. From Figure 3e, we can see that addition of methanol induces negligible current attenuation for Cu@NCNT/Co_xO_y composites, while current attenuation is pronounced for Pt/C catalysts. This implies that Cu@NCNT/Co_xO_y composites also have less sensitivity to impurities than do Pt/C catalysts.

Then, we studied the OER performance of pure CNTs, Cu@CNTs, Cu@NCNTs, and Cu@NCNT/Co_xO_y composites, by measuring their LSVs in oxygen saturated 0.1 M aq. KOH solution. As seen in Figure 3f, both pure CNTs and Cu@CNTs exhibit low current density (with a value far smaller than 10 mA cm^{-2}) under these conditions, but Cu@CNTs have a current density remarkably higher than that of pure CNTs. Therefore, this result confirms that embedding Cu gives rise to enhanced OER activity of pure CNTs, which agrees well with our expectation as well as Bao and co-workers's theoretical calculations.[42] In addition, the OER activities of Cu@CNTs, Cu@NCNTs, and Cu@NCNT/Co_xO_y composites increase in the following sequence Cu@CNTs < Cu@NCNTs < Cu@NCNT/Co_xO_y composites. As both pyridinic N and pyrrolic N as well as metal–N species favor the enhancement of OER activity of the carbon nanomaterials,[35,38] the higher OER activity of Cu@NCNTs than that of Cu@CNTs could be attributed to each of pyridinic N, pyrrolic N, and Cu–N species (the possible contribution of Cu–N species is revealed in Figure S11, Supporting Information). It has been evidenced that both CoO and Co_3O_4 have synergistic coupling with carbon nanomaterials to result in the efficiently improved OER activity of carbon nanomaterials.[37,41] Thus, we think the higher OER activity of the Cu@NCNT/Co_xO_y composites than that of Cu@NCNTs stems from synergistic coupling between cobalt oxide components (i.e., CoO and Co_3O_4 within Co_xO_y nanoparticles) and Cu@NCNTs. More importantly, Figure 3f shows that Cu@NCNT/Co_xO_y composites exhibit a current density of 10 mA cm^{-2} at ≈1.6 V, which is more negative than that (≈1.65 V) of the state-of-the-art (precious metal) IrO_2 catalysts. This reveals that Cu@NCNT/Co_xO_y composites are highly active OER catalysts. Moreover, chronoamperometric measurement at 1.47 V in oxygen saturated 0.1 M aq. KOH solution (Figure S12, Supporting Information) shows that Cu@NCNT/Co_xO_y composites still maintain ≈86% of their original current density after the measurement for 20 000 s, revealing that Cu@NCNT/Co_xO_y composites have strong durability during OER.

Finally, we applied our synthesis approaches to other composites, where NCNT walls were embedded with different metal nanoparticles and NCNT surfaces were decorated with other metal oxide nanoparticles. First, by performing low- and high-temperature CVD growth of CNTs on AAO pore walls loaded with nickel nitrate, followed by ammonia post-treatment and Co_xO_y decoration, we obtained Ni@NCNT/Co_xO_y composites, where NCNT walls were embedded with Ni nanoparticles. **Figure 4**a–c and Figure S13 (Supporting Information) show characterization results of the resulting Ni@NCNT/Co_xO_y composites. In comparison with Ni@CNTs (Figure 4d) achieved via only high-temperature CVD, we can see that Ni@NCNT/Co_xO_y composites have noticeably thicker CNT walls (CNT wall thicknesses for Ni@NCNT/Co_xO_y composites and Ni@CNTs are ≈6 and ≈3 nm, respectively). As ammonia post-treatment and Co_xO_y decoration processes induce no change in CNT wall thickness, this result reveals that the Ni@CNTs achieved via low- and high-temperature CVD have thicker walls than their counterparts fabricated via only high-temperature CVD. Therefore, this confirms again that the combination of low- and high-temperature CVD can favor the generation of thick-wall CNTs. In addition, Figure 4d shows clearly that there are many curly Ni-catalyzed small-diameter (≈5 nm) CNTs inside Ni@CNTs (marked by red arrows). This indicates that catalytic effects of

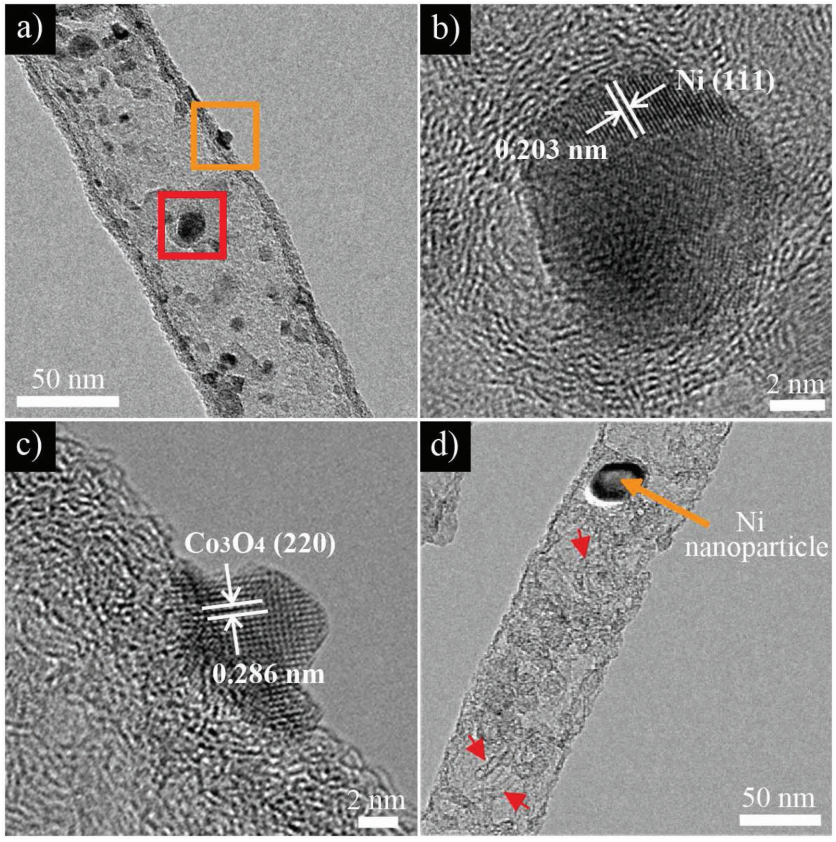

Figure 4. a) The TEM image of an Ni@NCNT/Co_xO_y composite. b,c) HRTEM images taken from the red and brown square areas in part (a), respectively. d) The TEM image of an Ni@CNT achieved by only high-temperature CVD. The red arrows indicate the Ni-catalyzed CNTs.

the Ni nanoparticles on CNT growth are primarily responsible for the formation of thin walls of the Ni@CNTs. Next, by precipitation-assisted separation of Cu@NCNTs from manganese nitrate and iron nitrate aqueous solutions, followed by thermal annealing, we fabricated Cu@NCNTs with surfaces decorated with manganese oxide (Mn_xO_y) and iron oxide (Fe_xO_y) nanoparticles. Figures S14 and S15 (Supporting Information) demonstrate characterization results of Cu@NCNT/Mn_xO_y (this Mn_xO_y is a mixture of MnO_2 and Mn_3O_4) and Cu@NCNT/Fe_xO_y composites (this Fe_xO_y is a mixture of Fe_3O_4, Fe_2O_3, and FeO), respectively. It can be observed that Mn_xO_y and Fe_xO_y nanoparticles are successfully decorated on the Cu@NCNT surfaces. It is noteworthy that other metal oxides (e.g., copper oxide, nickel oxide, and zinc oxide) can also be decorated on NCNT surfaces using similar methods.

3. Conclusions

In summary, we have demonstrated a novel synthetic protocol for the preparation of Cu@CNTs, in which Cu nanoparticles were embedded uniformly within the CNT walls, by consecutive low- and high-temperature CVD. This is, to our knowledge, the first report on utilization of this approach for controlled fabrication of metal–nanoparticle-embedded CNTs. In addition, this approach could deepen our understanding of the formation mechanism of CNTs and further benefit building of complex CNT-based functional nanoarchitectures. Then, we employed a rather simple, low-cost and eco-friendly approach to decoration of Cu@NCNT surfaces with Co_xO_y nanoparticles, via precipitation-assisted separation of Cu@NCNTs from cobalt nitrate aqueous solution and the subsequent thermal annealing. DFT calculations disclosed that the interaction of Cu nanoparticles with the surrounding CNT walls induced decreased work function of CNT surfaces and improved adsorption of hydroxyl ions onto the CNT surfaces. Hence, better ORR and OER activities of Cu@CNTs than pure CNTs were achieved. Owing to the combination of these merits with those from nitrogen doping and synergistic coupling between Co_xO_y nanoparticles and Cu@NCNTs, Cu@NCNT/Co_xO_y composites exhibited ORR catalytic activity similar to that of Pt/C catalysts and higher OER activity than IrO_2 catalysts. Moreover, these composites showed superior long-term stability for ORR/OER and strong tolerance to methanol crossover effect for ORR. Additionally, we obtained other composites consisting of different metal/metal oxide components using a similar approach, indicating that our approach is a general method for the fabrication of such metal@NCNT/metal oxide composites. Therefore, our strategy for the fabrication of Cu@NCNT/Co_xO_y composites may open a new option for designing high-performance carbon-based electrocatalysts with multifunctional catalytic activities for use in renewable energy technologies such as fuel cells and metal–air batteries.

4. Experimental Section

Fabrication of AAO: First, AAO films were fabricated via anodization at 40 V in 0.3 M oxalic acid at 10 °C for 15 h.[43,44] Then, pore widening of AAO was achieved by immersing AAO in a 10 wt% phosphoric acid aqueous solution at 30 °C for 15–20 min. Finally, copper nitrate was loaded on the AAO pore walls by immersing AAO in 0.8 M copper nitrate aqueous solution for 30 min, followed by drying.

Low- and High-Temperature CVD: The low-temperature CVD was conducted at 450 °C for 3 h with 50 sccm of C_2H_2 as precursor and 100 sccm of Ar as carrying gas.[22] The high-temperature CVD was carried out at 800 °C for 15 min with 10 sccm of C_2H_2 as precursor and 200 sccm of Ar as carrying gas.[22,45] Then, the Cu@CNTs were released from the AAO by dissolving the AAO in 10 M aq. NaOH at 90 °C for 20 h, followed by rinsing with deionized water for several times.

Nitrogen Doping: Cu@CNTs were first dispersed in water. Then, they were dropped onto silicon wafers and dried. Finally, the nitrogen doping was conducted at 900 °C for 30 min with 15 sccm of ammonia.[31]

Decoration of Co_xO_y Nanoparticles: First, the Cu@NCNTs were dispersed in cobalt nitrate aqueous solution. Then, the cobalt nitrate aqueous solution was sucked away via pipettes when most samples had precipitates at the bottom of the solution, leading to the separation of the Cu@NCNTs. In the next step, Cu@NCNTs which were encapsulated by residual cobalt nitrate aqueous solution were dried and annealed in Ar at 500 °C.

Characterizations: The SEM was performed on an FEI Nanonova 230, and the TEM and HRTEM were carried out on a JEOL JEM-2100F microscope (operated at 200 kV). The SEM specimen was prepared by dropping well-dispersed samples in ethanol on a silicon surface, and TEM (HRTEM) specimen was prepared by dropping well-dispersed samples in ethanol on carbon microgrids (Ted Pella, Inc., 200 Mesh Copper Grid). XPS spectra were recorded on a Thermo Fisher K-alpha XPS spectrometer. XRD patterns were recorded with a Rigaku D/MAZX 2500V/PC with Cu Kα radiation (35 kV, 20 mA, λ = 1.5418 Å). The nitrogen adsorption–desorption isotherm was measured by a surface area and porosity analyzer (Omnisorp 100CX), and the ICP-OES measurement was conducted on ICP 6300 (Thermo Fisher Scientific).

Electrochemical Measurements: The electrochemical tests were conducted on an electrochemical workstation (CHI 760D, CH Instruments, Inc., Shanghai, China) coupled with a PINE rotating disk electrode (RDE) system (Pine Instruments Co. Ltd, USA). A standard three-electrode electrochemical cell was used during measurements. A platinum wire and an Ag/AgCl (3 M KCl filled) electrode were used as counter and reference electrodes, respectively. The working electrodes were prepared by dropping catalyst ink onto the rotating disk electrodes (4 mm in diameter). Briefly, samples (5 mg) were dispersed in a mixture of ethanol (900 µL) and nafion (0.5 wt%, 100 µL), followed by ultrasonication for 5 min. Then, 8 µL of catalyst ink (which contained ≈40 µg of catalysts) was cast onto the surfaces of rotating disk electrodes, followed by drying at room temperature. In addition, the amount of each reference catalyst (Pt/C or IrO_2) loaded on the surface of a rotating disk electrode was also 40 µg. Furthermore, all the potential values used in the electrochemical measurements were transformed to those with respect to the RHE.

The detailed kinetic analysis was conducted according to the K–L plots

$$\frac{1}{j} = \frac{1}{j_k} + \frac{1}{B\omega^{0.5}} \quad (1)$$

where j_k is the kinetic current, ω is the electrode rotation rate, and B is the Levich slope which is given by

$$B = 0.2nF(D_{O_2})^{2/3}\nu^{-1/6}C_{O_2} \quad (2)$$

Here n is the number of electrons transferred during reduction of each oxygen molecule, F is the Faraday constant (F = 96 485 C mol^{-1}), D_{O_2} is the diffusion coefficient of oxygen in 0.1 M aq. KOH ($D_{O_2} = 1.9 \times 10^{-5}$ cm^2 s^{-1}), ν is the kinetic viscosity (ν = 0.01 cm^2 s^{-1}), and C_{O_2} is concentration of oxygen in the solution ($C_{O_2} = 1.2 \times 10^{-6}$ mol cm^{-3}). Therefore, according to Equations (1) and (2), n can be obtained from the slope of the K–L plot (j^{-1} vs $\omega^{-1/2}$).

Supporting Information

Supporting Information is available from the Wiley Online Library or from the author.

Acknowledgements

This work was supported by the Creative Research Initiative (CRI, 2014R1A3A2069102), BK21 PLUS (10Z20130011057) and Science Research Center (SRC, 2016R1A5A1009405) programs through the National Research Foundation (NRF) of Korea. Also, the authors thank the National Natural Science Foundation of China (Grant No. 11547170) for financial support.

Received: November 1, 2016
Revised: December 7, 2016
Published online: January 18, 2017

[1] M. Winter, R. J. Brodd, *Chem. Rev.* **2004**, *104*, 4245.
[2] J. Suntivich, K. J. May, H. A. Gasteiger, J. B. Goodenough, Y. Shao-Horn, *Science* **2011**, *334*, 1383.
[3] Z. Peng, H. Yang, *J. Am. Chem. Soc.* **2009**, *131*, 7542.
[4] M. E. G. Lyons, S. Floquet, *Phys. Chem. Chem. Phys.* **2011**, *13*, 5314.
[5] J. Duan, S. Chen, A. Vasileff, S. Z. Qiao, *ACS Nano* **2016**, *10*, 8738.
[6] J. Suntivich, H. A. Gasteiger, N. Yabuuchi, H. Nakanishi, J. B. Goodenough, Y. Shao-Horn, *Nat. Chem.* **2011**, *3*, 546.
[7] F. Cheng, J. Shen, B. Peng, Y. Pan, Z. Tao, J. Chen, *Nat. Chem.* **2011**, *3*, 79.
[8] K. Gong, F. Du, Z. Xia, M. Durstock, L. Dai, *Science* **2009**, *323*, 760.
[9] Y. Zhao, L. Yang, S. Chen, X. Wang, Y. Ma, Q. Wu, Y. Jiang, W. Qian, Z. Hu, *J. Am. Chem. Soc.* **2013**, *135*, 1201.
[10] J. Liang, Y. Jiao, M. Jaroniec, S. Z. Qiao, *Angew. Chem.* **2012**, *124*, 11664; *Angew. Chem. Int. Ed.* **2012**, *51*, 11496.
[11] I. Jeon, M. Choi, H. Choi, S. Jung, M. Kim, J. Seo, S. Bae, S. Yoo, G. Kim, H. Y. Jeong, N. Park, J. Baek, *Nat. Commun.* **2015**, *6*, 7123.
[12] J. Duan, S. Chen, M. Jaroniec, S. Z. Qiao, *ACS Catal.* **2015**, *5*, 5207.
[13] K. Qu, Y. Zheng, S. Dai, S. Z. Qiao, *Nano Energy* **2016**, *19*, 373.
[14] B. Bayatsarmadi, Y. Zheng, Y. Tang, M. Jaroniec, S. Qiao, *Small* **2016**, *12*, 3703.
[15] Z. Yang, X. Zhou, Z. Jin, Z. Liu, H. Nie, X. Chen, S. Huang, *Adv. Mater.* **2014**, *26*, 3156.
[16] J. Duan, S. Chen, S. Dai, S. Z. Qiao, *Adv. Funct. Mater.* **2014**, *24*, 2072.
[17] Z. Wu, S. Yang, Y. Sun, K. Parvez, X. Feng, K. Müllen, *J. Am. Chem. Soc.* **2012**, *134*, 9082.
[18] M. Sun, Y. Dong, G. Zhang, J. Qu, J. Li, *J. Mater. Chem. A* **2014**, *2*, 13635.
[19] Y. Liang, H. Wang, P. Diao, W. Chang, G. Hong, Y. Li, M. Gong, L. Xie, J. Zhou, J. Wang, T. Z. Regier, F. Wei, H. Dai, *J. Am. Chem. Soc.* **2012**, *134*, 15849.
[20] D. Deng, L. Yu, X. Chen, G. Wang, L. Jin, X. Pan, J. Deng, G. Sun, X. Bao, *Angew. Chem.* **2013**, *125*, 389; *Angew. Chem. Int. Ed.* **2013**, *52*, 371.
[21] Z. Wu, Y. Li, J. Liu, Z. Lu, H. Zhang, B. Yang, *Angew. Chem.* **2014**, *126*, 12392; *Angew. Chem. Int. Ed.* **2014**, *53*, 12196.
[22] X. Zhao, G. Meng, F. Han, X. Li, B. Chen, Q. Xu, X. Zhu, Z. Chu, M. Kong, Q. Huang, *Sci. Rep.* **2013**, *3*, 2238.
[23] C. Klinke, J. Bonard, K. Kern, *Phys. Rev. B* **2005**, *71*, 035403.
[24] M. Cantoro, S. Hofmann, S. Pisana, V. Scardaci, A. Parvez, C. Ducati, A. C. Ferrari, A. M. Blackburn, K. Wang, J. Robertson, *Nano Lett.* **2006**, *6*, 1107.
[25] G. Che, B. B. Lakshmi, C. R. Martin, E. R. Fisher, R. S. Ruoff, *Chem. Mater.* **1998**, *10*, 260.
[26] G. Meng, Y. J. Jung, A. Cao, R. Vajtai, P. M. Ajayan, *Proc. Natl. Acad. Sci. USA* **2005**, *102*, 7074.
[27] H. Chun, M. G. Hahm, Y. Homma, R. Meritz, K. Kuramochi, L. Menon, L. Ci, P. M. Ajayan, Y. J. Jung, *ACS Nano* **2009**, *3*, 1274.
[28] J. Li, C. Papadopoulos, J. Xu, *Nature* **1999**, *402*, 253.
[29] F. S. Ou, M. M. Shaijumon, L. Ci, P. M. Ajayan, *Carbon* **2007**, *45*, 1696.
[30] C. Chen, A. Ogino, X. Wang, M. Nagatsu, *Appl. Phys. Lett.* **2010**, *96*, 131504.
[31] T. C. Nagaiah, S. Kundu, M. Bron, M. Muhler, W. Schuhmann, *Electrochem. Commun.* **2010**, *12*, 338.
[32] X. Zhao, G. Meng, Q. Xu, F. Han, Q. Huang, *Adv. Mater.* **2010**, *22*, 2637.
[33] C. Navío, M. J. Capitán, J. Álvarez, F. Yndurain, R. Miranda, *Phys. Rev. B* **2007**, *76*, 085105.
[34] J. Hao, Y. Liao, Y. Zhong, D. Shu, C. He, S. Guo, Y. Huang, J. Zhong, L. Hu, *Carbon* **2015**, *94*, 879.
[35] S. Chen, J. Duan, M. Jaroniec, S. Qiao, *Adv. Mater.* **2014**, *26*, 2925.
[36] H. Wu, H. Li, X. Zhao, Q. Liu, J. Wang, J. Xiao, S. Xie, R. Si, F. Yang, S. Miao, X. Guo, G. Wang, X. Bao, *Energy Environ. Sci.* **2016**, *9*, 3736.
[37] Y. Liang, Y. Li, H. Wang, J. Zhou, J. Wang, T. Regier, H. Dai, *Nat. Mater.* **2011**, *10*, 780.
[38] Y. Hou, M. Qiu, T. Zhang, J. Ma, S. Liu, X. Zhuang, C. Yuan, X. Feng, *Adv. Mater.* **2016**, DOI: 10.1002/adma.201604480.
[39] T. Ling, D. Yan, Y. Jiao, H. Wang, Y. Zheng, X. Zheng, J. Mao, X. Du, Z. Hu, M. Jaroniec, S. Qiao, *Nat. Commun.* **2016**, *7*, 12876.
[40] J. Wu, Y. Xue, X. Yan, W. Yan, Q. Cheng, Y. Xie, *Nano Res.* **2012**, *5*, 521.
[41] S. Mao, Z. Wen, T. Huang, Y. Hou, J. Chen, *Energy Environ. Sci.* **2014**, *7*, 609.
[42] X. Cui, P. Ren, D. Deng, J. Deng, X. Bao, *Energy Environ. Sci.* **2016**, *9*, 123.
[43] H. Masuda, M. Satoh, *Jpn. J. Appl. Phys.* **1996**, *35*, L126.
[44] B. Chen, Q. Xu, X. Zhao, X. Zhu, M. Kong, G. Meng, *Adv. Funct. Mater.* **2010**, *20*, 3791.
[45] W. Xu, T. Kyotani, B. K. Pradhan, T. Nakajima, A. Tomita, *Adv. Mater.* **2003**, *15*, 1087.